RESEARCH ARTICLE

Relationships between shear strength parameters and microstructure of alkaline-contaminated red clay

Qi Wang[1] · Jun Chen[2] · Jiankun Liu[1,3,4] · Mingyuan Yu[1] · Weijuan Geng[3] · Pengcheng Wang[5] · Zhonghu Wu[6]

Abstract

The leachate (pH = 14) from alumina production changes the mechanical properties of red clay, and the shear strength parameters of the system vary due to the multiple-dimensional interactions of the microscopic parameters. In this paper, the alumina production liquid and the concentrations of the NaOH solution were designed to contaminate the red clay during 80 days. The cohesion and friction angle of the alkaline-contaminated red clay were obtained from direct shear tests. Through qualitative and quantitative analyses using scanning electron microscopy (SEM), the microstructure was observed. Based on the rock engineering systems (RES) theory, interactions among microscopic parameters were analysed, and the relationships between shear strength parameters and microscopic parameters of alkaline-contaminated red clay were established. Results show that both of the cohesion and friction angle of alkaline-contaminated red clay are increased in general; the adsorption in alumina production liquid and dispersing effect of 0.7% NaOH concentration are noticeable, and the interactions of the microscopic parameters are intense; the ratio of the intra-aggregate pore number, the probability distribution index and the number of particles can significantly influence cohesion; the particle morphology fractal dimension, aspect and probability entropy have a severe effect on friction angle. This work is expected to serve as a reference for future research on the relationship between macroscopic properties and microcosmic structure of soil.

Keywords Alkaline-contaminated red clay · Cohesion · Friction angle · Microstructure · Rock engineering systems

Introduction

Leachate is a hazardous liquid and can even lead to security incidents in many chemical plants. The seepage action of

✉ Jiankun Liu
liujiank@mail.sysu.edu.cn

1 School of Civil Engineering, Beijing Jiaotong University, Beijing 100044, China

2 Guizhou Institute of Technology, Guiyang 550007, China

3 School of Civil Engineering, Sun Yat-sen University, Guangzhou 510006, China

4 Southern Marine Science and Engineering Guangdong Laboratory, Zhuhai, China

5 Railway Engineering Research Institute, China Academy of Railway Sciences Corporation Limited, Beijing 100081, China

6 College of Civil Engineering, Guizhou University, Guiyang 550025, China

leachate always increases the pH values of soils, and minerals are likely to undergo physicochemical transformations under a high-pH environment (Cuisinier et al. 2009). Leachate makes the stability of the engineering property of the foundation soil decrease, and prolonged contamination also changes the shear strength of the soil (Sunil et al. 2009; Ratnaweera and Meegoda 1991; Rosli et al. 2019). To reveal the changes of macroscopic properties, many studies have researched on the microstructures and relationship between macroscopic properties and the microcosmic structure of the soil (Anandarajah and Kuganenthira 1995; Pusch and Weston 2003; Cox and Budhu 2008), including quantitative analysis or mineral change (Thomas et al. 2018; Reig et al. 2013; Sedira et al. 2018; Reddy and Sivapullaiah 2010; Chavali et al. 2016). Ratnaweera and Meegoda (1991) proposed that the pore fluid viscosity of the contaminated soil is responsible for the degradation of the shear strength. Chen et al. (2019) reported that the finer pore size distribution, larger-sized particles, aggregated and a flocculent network of clay are occured after nZVI contaminated.

In fact, the soil properties are influenced not by the independent variables but by the simultaneous couplings among all the variables; however, it is rarely discussed. A rock

engineering system (RES) is used to realize the simultaneous couplings of variables in rock, which is one of the most powerful methods in rock engineering for solving complex engineering problems (Huang et al. 2013; Jiao and Hudson 1995; Hudson 1992), and it has been used for a wide variety of other problems (Hudson 2013). Therefore, RES is also applicable in the analysis of simultaneous couplings of variables in soil.

Fresh red clay in Guizhou Province was used in this study; it was contaminated by different concentrations and kinds of alkaline solution for 80 days in the laboratory, after which the changes of macroscopic and microscopic properties of the alkaline-contaminated red clay were studied, and 9 microscopic parameters were quantitatively analysed. Then, based on RES theory, considering the simultaneous couplings among microscopic parameters, a back-propagation (BP) neural network was used to study the interaction matrix among nine parameters, and the weightings of the microscopic parameters on cohesion and friction angle were obtained, respectively. This work is expected to reveal the variable features of the soil microstructure after alkaline contamination, and serves as a reference for future research on the relationship between macroscopic properties and microcosmic structure of soil, and tries to provide theoretical support for amending the soil at the microscopic level.

Materials and methodology

The alumina production plant investigated in this work was built in 1958 in Guiyang area, the central area of Guizhou Province. Because concrete pipes were broken (Fig. 1a), leachate from alumina production (Fig. 1d–f) infiltrated into the foundation soil (Fig. 1b) and contaminated the red clay beneath the plant (Fig. 1c). The pH value of leachate from alumina production is 14. The colour of the red clay changed from red to grey.

Materials

The sampling area is located in Guiyang area, China. The underlying formation of red clay in this work is the medium-weathered dolomite of the Anshun formation of the Lower Triassic. The sampling area was not contaminated by alkaline leachate; the undisturbed and fresh red clay was used in this study. The samples were cured in the concentrations of 0.7%, 3.8%, 7%, 14%, and 21% NaOH solution and alumina production liquid (Fig. 1d, Table 1) for 10, 20, 40, and 80 days, respectively. Group samples were cured in deionized water as a reference. The NaOH solution was prepared with deionized water and sodium hydroxide of reagent grade with a purity of at least 99%. The chemical composition of alumina production liquid is shown in Table 1. SiO$_2$

was measured by spectrophotometry (Ministry of Water Resources of the People's Republic of China 1994), organic matter content was tested by a mixture of potassium bichromate solution and sulphuric acid (Ministry of Agriculture of the People's Republic of China 1988), Al$_2$O$_3$ was measured by complexometric titration (GBAC 2013a), Na$_2$O$_k$ was measured by acid-base titration (GBAC 2013b), and the sum of Na$_2$O$_k$ and Na$_2$O$_c$ were measured by acid-base titration; thus, the content of Na$_2$O$_c$ can be calculated (GBAC 2013a).

The density (ring knife method), specific gravity (pycnometer method), water content (drying method), plasticity (liquid and plastic limit water content joint measurement) and coefficient of compressibility (standard consolidation test) of contaminated red clay were tested (China Water Power Press 1999). Organic matter content was tested by a mixture of potassium dichromate solution and sulphuric acid (Ministry of Agriculture of the People's Republic of China 1988). Particle size analysis was tested by the laser particle size analyser (BT-9300H, China), and the particles less than 5 μm are regarded as clay (Editorial Committee of Handbook of Engineering Geology 2017). The void ratio (e) was calculated by density of soil (ρ_0) and water (ρ_w), specific gravity (G_s) and water content (ω_0) (Eq. 1). The physics and mechanics properties of alkaline-contaminated red clay are shown in Table 2.

$$e = \frac{\rho_w G_s (1 + 0.01\omega_0)}{\rho_0} - 1 \tag{1}$$

Direct shear test

The cohesion and friction angle of the alkaline contaminated red clay were obtained from direct shear test under normal stress of 100 kPa, 200 kPa, 300 kPa and 400 kPa, respectively (China Water Power Press 1999). Two or three parallel samples were set up for each specimen to ensure the testing data are reliable.

Microscopic tests

The fracture surface where shear displacement reached 4 mm under 300 kPa consolidation pressure in the direct shear test was cut to 1.5 cm × 1.5 cm × 1 cm. After drying in air, the soil cube was taken to observe the morphology of minerals by scanning electronic microscope (Zeiss ΣIGMA+X-Max20, Germany).

Fig. 1 The alumina production plant after alkaline infiltration: **a** ruptured concrete pipe in the alumina production plant; **b** leachate infiltrated into the foundation red clay; **c** the contaminated the red clay. Leachate from alumina production: According to calculations, sodium ions are provided by NaOH: **d** the alumina production liquid; **e** leachate from the no. 3 foundation pit; **f** leachate from the no. 1 foundation pit
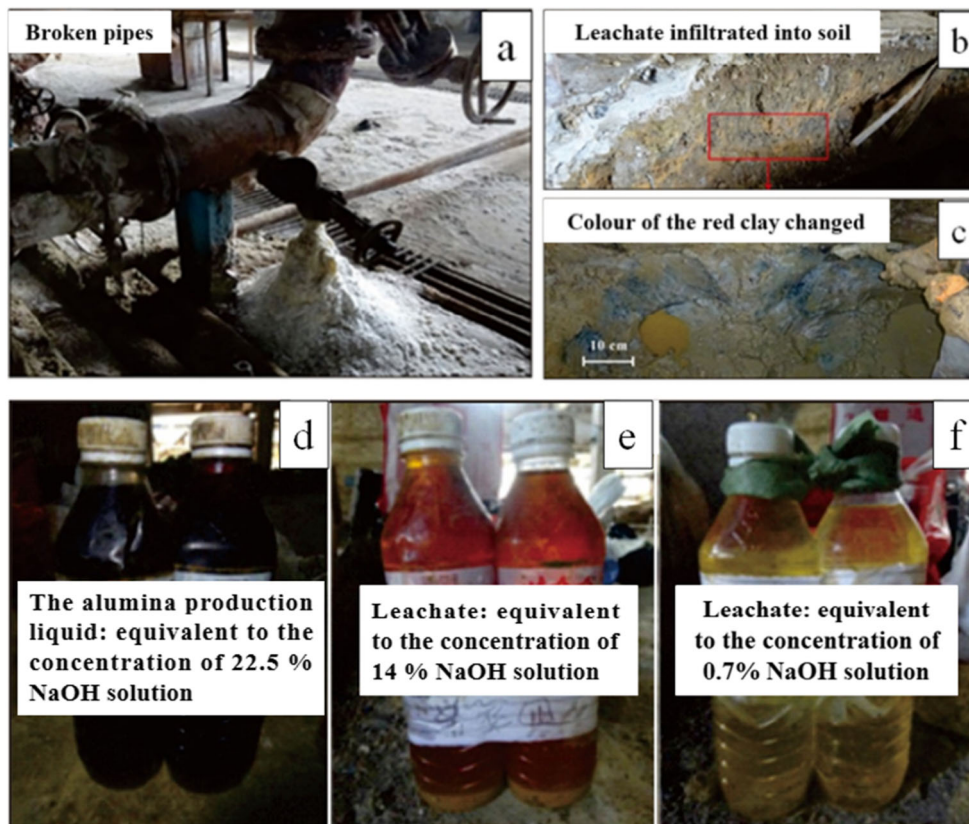
Computation method

Selection of microscopic parameters

The microscopic parameters were extracted from the scanning electron microscope (SEM) through Particles (Pores) and Cracks Analysis System (PCAS) and Image-Pro plus (IPP). A total of nine microscopic parameters of the soil were initially judged as the main factors leading to cohesion and friction angle.

(1) Total number of pores, total pore area, particle morphology fractal dimension, the number of particles, aspect (the ratio between the minor axis and major axis of the ellipse equivalent to a particle; the larger the value, the rounder the particle), probability entropy (describing the directionality of the main axis of the ellipse equivalent to a pore; the smaller the value, the more orderly the arrangements of the pores' direction) and probability distribution index (representing the density of the pores in a

given area; the larger the value, the smaller the pores) (Liu et al. 2011).

(2) The ratio of the intra-aggregate pore area and the ratio of the intra-aggregate pore number. There are two types of pores in the soil: intra-aggregate pore (pores inside the soil aggregates) and inter-aggregate pore (pores among the aggregates) (Chertkov 2008). Under the same pressure, the volume and quantity of inter-aggregate pores would be easier to decrease than those of the intra-aggregate pores. Because the particle with a diameter less than 5 μm is classified as clay (Editorial Committee of Handbook of Engineering Geology 2017), in this paper, a pore with a diameter of less than 5 μm was similarly regarded as an intra-aggregate pore. Assuming that the total pore area was S and the intra-aggregate pore area was S_1, the ratio of the intra-aggregate pore area was S_1/S. Assuming that the total number of pores was N and the number of intra-aggregate pore was N_1, the ratio of the intra-aggregate pore number was N_1/N.

Table 1 Chemical composition of the alumina production liquid

Composition	Na_2O_k	Na_2O_c	Al_2O_3	SiO_2	Organic matter
Content (g L^{-1})	240.00	36.80	142.10	1.00	1.50

Table 2 Properties of alkaline-contaminated red clay

Sample	Properties							
	Density (kg cm^{-3})	Organic matter content (g kg^{-1})	Clay content (%)	Specific gravity	Water content ω(%)	Void ratio, e	Plasticity index, I_P	Coefficient of compressibility, a_{1-2} (MPa^{-1})
Fresh undisturbed red clay	1.851	44.900	44.38	2.68	41.93	1.054	30.07	0.63
0.7%, 10 days	1.861	40.446	54.66	2.71	43.28	1.083	25.40	0.525
0.7%, 20 days	1.842	37.325	58.63	2.71	41.66	1.085	24.66	0.502
0.7%, 40 days	1.834	35.227	61.13	2.73	37.95	1.058	26.25	0.454
0.7%, 80 days	1.803	34.516	54.13	2.53	46.22	1.056	27.62	0.449
3.8%, 10 days	1.827	35.657	51.55	2.70	37.28	1.028	33.23	0.252
3.8%, 20 days	1.864	31.338	46.21	2.61	46.27	1.045	27.61	0.144
3.8%, 40 days	1.932	28.599	45.17	2.68	42.03	0.968	24.57	0.242
3.8%, 80 days	1.925	26.909	40.8	2.74	44.59	1.058	28.77	0.341
7%, 10 days	1.916	32.269	57.79	2.69	42.53	1.001	31.17	0.275
7%, 20 days	1.941	26.637	47.84	2.62	51.84	1.052	27.15	0.286
7%, 40 days	1.834	24.242	41.22	2.54	45.24	1.009	23.59	0.508
7%, 80 days	1.770	22.249	38.82	2.59	51.63	1.220	26.70	0.507
14%, 10 days	1.989	31.920	60.35	2.72	43.49	0.960	35.11	0.329
14%, 20 days	1.874	24.840	50.27	2.68	44.51	1.069	28.73	0.527
14%, 40 days	1.826	23.734	38.83	2.54	48.79	1.065	22.53	0.618
14%, 80 days	1.803	22.977	31.71	2.69	49.99	1.235	25.10	0.561
21%, 10 days	2.041	29.572	65.57	2.72	45.82	0.944	38.12	0.436
21%, 20 days	1.942	25.233	43.86	2.68	45.52	1.005	24.50	0.506
21%, 40 days	1.876	23.199	32.97	2.56	45.16	0.984	21.41	0.365
21%, 80 days	1.874	22.314	30.13	2.67	47.91	1.105	24.01	0.534
Alumina production liquid, 10 days	2.052	42.890	35.83	2.80	35.14	0.842	17.75	0.198
Alumina production liquid, 20 days	1.989	40.958	38.59	2.66	38.07	0.846	13.49	0.132
Alumina production liquid, 40 days	2.006	34.346	30.92	2.60	35.54	0.756	16.50	0.201
Alumina production liquid, 80 days	1.997	31.000	27.17	2.53	29.13	0.639	14.07	0.237

Application of RES

Soil is a coupled, nonlinear and dynamic system in which the change of the shear strength parameters depends on the multiple-dimensional interaction of the microscopic parameters. The internal effect of one microscopic parameter and the external effect resulting from the interaction between any two micro-parameters would influence the shear strength parameter. RES (Hudson 1992) is a suitable method to analyse these influences.

The interaction matrix is the basic analytical device used in the RES approach for considering all variables relevant to a particular engineering problem (Hudson and Harrison 1992). In RES, all factors affecting the shear strength parameters are arranged along the leading diagonal of the interaction matrix.

Off-diagonal position is in correspondence with the influence degree of one specific individual factor on any another factor, as shown in Table 3.

At present, the BP network is often used to construct the ANN coding of the RES interaction matrix (Yang and Zhang 1998; Meulenkamp and Alvarez Grima 1999; Singh et al. 2001). It could quantitatively evaluate the influence and interaction intensity of microscopic parameters on shear strength

Table 3 The principle of the interaction matrix (Hudson 1992)

A	Influence of A on B	Influence of A on C
Influence of B on A	B	Influence of B on C
Influence of C on A	Influence of C on B	C

parameters of soil. A BP network with three layers was used to illustrate the influence of the input on the output (Fig. 2).

Network establishing

Parameter setting

The cohesion and the friction angle of soil were designated as Y_1 and Y_2, respectively. The microscopic parameters, including the particle morphology fractal dimension, aspect, total number of pores, ratio of the intra-aggregate pore area, ratio of the intra-aggregate pore number, total pore area, probability distribution index, probability entropy, and number of particles, were designated as X_1, X_2, ..., X_8, X_9, respectively. From the laboratory tests, 25 sets of experimental data were obtained. The serial number of 1 to 25 in the left column represented the red clays cured in various solutions for different days: fresh undisturbed red clay, red clays cured in a concentration of 0.7% NaOH for 20 days, 0.7% NaOH for 40 days, 0.7% NaOH for 80 days, 3.8% NaOH for 10 days, 3.8% NaOH for 40 days, 3.8% NaOH for 80 days, 7% NaOH for 10 days, 7% NaOH for 20 days, 7% NaOH for 80 days, 14% NaOH for 10 days, 14% NaOH for 20 days, 14% NaOH for 40 days, 21% NaOH for 10 days, 21% NaOH for 20 days, 21% NaOH for 40 days, alumina production liquid for 10 days, alumina production liquid for 40 days, alumina production liquid for 80 days, 0.7% NaOH for 10 days, 3.8% NaOH for 20 days, 7% NaOH for 40 days, 14% NaOH for 80 days, 21% NaOH for 80 days, and alumina production liquid for 20 days,
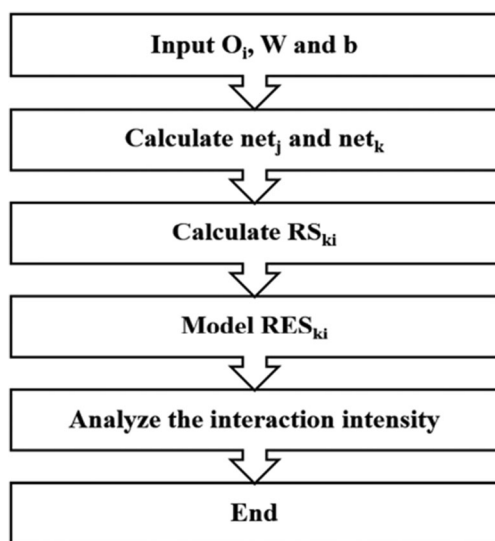

Fig. 2 Process of RES algorithm implementation based on the BP neural network: O_i, W, b, net$_j$, net$_k$, RS$_{ki}$ and RES$_{ki}$ represent the input node of the input layer, weight, threshold, output node of the hidden layer, input node of the output layer, intensity of input on output and interaction matrix, respectively

respectively. The former nineteen sets were used for training, and the latter six sets were used for prediction.

Network training

All the dates of each column were divided by the maximum value of that column to normalize the dates (Mulak et al. 2016). After the normalization, the experimental data of all of the 25 sets were in the interval between 0 and 1 (Table 4).

The logarithmic sigmoid function of the BP network for layer-to-layer construction was used to achieve the coding of the interaction matrix, the process of weight calculation and the coding of the RES matrix (Ma et al. 2006). An algorithm model of the RES matrix based on the BP neural network was established in MATLAB. The functions both of the input layer to the hidden layer and the hidden layer to the output layer were logsig: $f(x) = 1/(1 + \exp(-x))$. The Levenberg-Marquardt algorithm was used for training the trainlm function; the output error is less than 0.1.

Results and discussion

Shear strength parameters

Cohesion

From Fig. 3, it can be seen that the cohesion of samples increased to its peak value during the tenth day to the fortieth day and then decreased to stable during the fortieth day to the eightieth day. Compared with the cohesion of soils cured in deionized water, the cohesion of alkaline-contaminated red clays is increased, in which the cohesion of clays cured in alumina production liquid is the largest. And the cohesion of the samples cured in NaOH solution is between the value of deionized water and alumina production liquid.

Friction angle

It can be seen from Fig. 4 that the friction angle is increased to its peak value during the tenth day to the twentieth day, and then decreased at about the fortieth day, and finally increased to stable at about the eightieth day. Compared with the friction angle of soils cured in deionized water, the friction angle of alkaline-contaminated red clays is increased generally, in which the friction angles of clays cured in 0.7% NaOH solution are the lowest and those of clays cured in alumina production liquid are the largest generally.

Microstructure analysis

The microstructures of soil were analysed, as shown in Fig. 5.

Table 4　Sample normalization of 25 sets of experimental data

Sample	Y_1	Y_2	X_1	X_2	X_3	X_4	X_5	X_6	X_7	X_8	X_9
1	0.141	0.635	0.952	0.947	0.887	0.276	0.739	0.958	0.776	1.000	0.626
2	0.249	0.336	0.951	0.940	0.605	0.230	0.686	0.982	0.654	0.991	0.910
3	0.370	0.380	0.946	0.906	0.641	0.244	0.705	0.972	0.680	0.989	0.959
4	0.228	0.504	0.943	0.927	0.641	0.245	0.713	0.963	0.687	0.986	0.770
5	0.191	0.811	0.971	0.955	0.793	0.489	0.937	0.955	0.784	0.986	0.805
6	0.692	0.579	0.955	0.902	0.903	0.505	0.807	0.958	0.801	0.986	0.499
7	0.263	0.677	0.948	0.929	1.000	0.502	0.767	0.941	0.799	0.985	0.464
8	0.439	0.725	0.975	0.973	0.834	0.511	0.953	0.949	0.832	0.995	0.830
9	0.335	0.773	0.967	0.909	0.918	0.534	0.847	0.912	0.832	0.992	0.544
10	0.341	0.770	0.909	0.912	0.939	0.494	0.863	0.968	0.800	0.984	0.404
11	0.328	0.709	0.979	0.985	0.947	0.539	0.910	0.923	0.808	0.983	0.816
12	0.378	0.655	0.959	0.924	0.937	0.559	0.910	0.893	0.835	0.989	0.664
13	0.238	0.788	0.932	0.894	0.895	0.545	0.963	0.933	0.833	0.984	0.410
14	0.231	0.803	1.000	0.990	0.979	0.392	0.932	0.915	0.938	0.985	1.000
15	0.333	0.627	0.891	0.891	0.597	0.308	1.000	0.949	0.894	0.990	0.671
16	0.332	0.665	0.855	0.885	0.381	0.429	0.999	0.942	0.834	0.986	0.335
17	1.000	0.751	0.974	1.000	0.651	1.000	0.996	0.868	1.000	0.996	0.341
18	0.675	0.930	0.882	0.869	0.445	0.608	0.995	0.805	0.992	0.981	0.331
19	0.675	0.930	0.879	0.824	0.434	0.744	0.995	0.735	0.996	0.973	0.283
20	0.105	0.325	0.966	0.967	0.642	0.258	0.639	0.978	0.660	0.996	0.780
21	0.323	0.749	0.972	0.943	0.909	0.516	0.848	0.955	0.798	0.987	0.606
22	0.188	0.786	0.914	0.915	0.924	0.524	0.858	0.936	0.818	0.987	0.432
23	0.200	0.858	0.910	0.900	0.953	0.532	0.856	0.980	0.811	0.983	0.375
24	0.059	0.853	0.874	0.878	0.412	0.416	0.986	1.000	0.813	0.982	0.333
25	0.430	1.000	0.866	0.882	0.513	0.576	0.999	0.856	0.942	0.990	0.360

From Fig. 5a, both of the particles and pores are distributed randomly, and the particle size is larger. And the particles of red clay were presented in a sheet-like shape and a rough surface (Fig. 5b). Under the attack of NaOH solution, on the
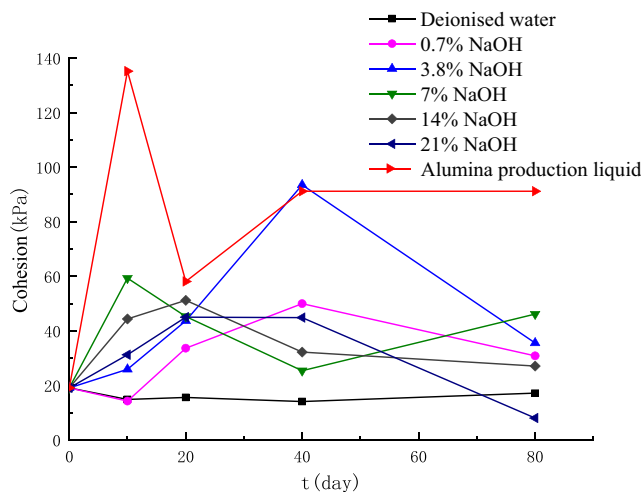

Fig. 3 Cohesion curves for samples with various concentrations of NaOH solution over time

whole, the cohesion was increased and then finally decreased to a stable stage. In the early stage of reaction (in the first 10 days), compared with Fig. 5a, Fig. 5c was arranged more closely. This is because there were many aluminium and iron elements in red clay, which reacted with NaOH and formed the spherical-like new salts (Fig. 5d), for example, Na_2SiO_3, $Al(OH)_3$ and $Fe(OH)_2$ (Fig. 5q). The particle regions and the number of small-size pores increased; thus, the individual particles were arranged and connected more closely, and resulted in the increase of cohesion. Because the salts were covering the surface of particles, the surfaces of particles became rougher, and the resulting friction angle increased.

In the middle stage of reaction (after day 10 to day 40), due to the adsorption of clay minerals (Yin et al. 2005), it can be seen that a large number of substances were absorbed by particles, in the shape of the block-like and covering the surface of particles (Fig. 5f, h). The area of the adsorbate was S_a, and the total area of the SEM was S. The proportion of the adsorbate was S_a/S, and the proportion of adsorbates of Fig. 5e, g were measured about 40% and 27%, respectively. The adsorbates made the contacts between particles increase, and resulted in an increase in the cohesion of soil. In this stage, the new

Fig. 4 Friction angle curves for samples with various concentrations of NaOH solution over time
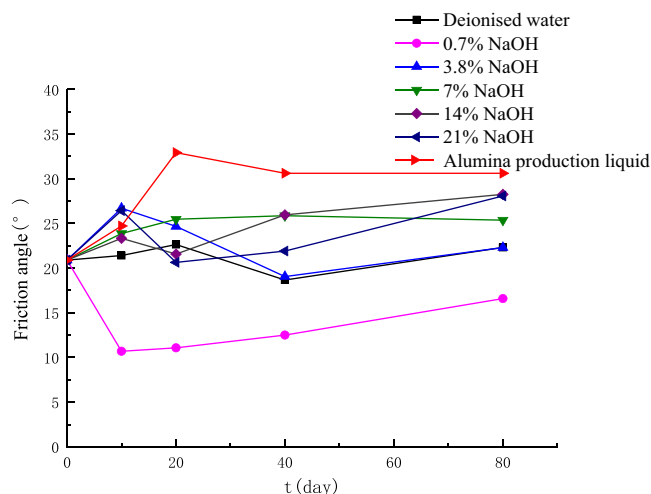
salts dissolved and migrated; meanwhile, particles reacted with NaOH solution continually, and the new bond formed filling between particles. It is worth noticing that the adsorption always existed in this stage, and the reactions of new salts dissolved and new bond formed were not completely separate but maybe simultaneously. If the sum of the influences of adsorption and new bond formed were stronger than the new salts dissolved, the cohesion would be increased, and vice versa. At the early period of the middle stage (after day 10 to day 20), the sum of the effects of adsorption and new bond formed were stronger than the new salts dissolved, which made the internal bond among soils increase and resulted in increased cohesion (Fig. 5e). And the surface of particles became smooth due to the new bond generated, leading to the decreased of the friction angle generally. At the later period of the middle stage (after day 20 to day 40), the effect of new salts dissolved was greater than the sum of the adsorption and new bond formed, thus resulting in decreased cohesion (Fig. 5g). The salts dissolved also made the surface of particles rough, and resulted in the increase of the friction angle generally. Because the concentrations of NaOH solution were different, the simultaneous influence among adsorption, new salts dissolved and new bond formed was also different between the reaction of red clay and NaOH solution. Thus, the cohesion of the specimens cured in NaOH solution reached a peak value at the different time and then decreased in the whole middle stage. Due to low concentration of 0.7% and 3.8% NaOH solution, the reaction rate between soils and solution was slower; thus, the cohesion of the soil reached the peak value at 40 days, then decreased.

Finally (after day 40 to 80), the bond was dissolved to form the soluble salts and reached the ionic equilibrium, the pores extended and the surfaces of particles became rough (Fig. 5i), so the cohesion reduced and the friction angle increased.

However, the friction angle of contaminated red clay cured in a concentration of 0.7% NaOH was decreased. In the particle analysis experiment, sodium hydroxide can be used as disperser (Ministry of Transport of the People's Republic of China 2007). Through experimental tests performed many times, it was found that the dispersing effect is better at a concentration of 0.7% NaOH than at 3.8%, 7%, 14%, and 21% NaOH, respectively. And the surface of the particle became smooth and attraction of the particles were decreased; therefore, the dispersing effect may be the main reason for big-size pores formed (Fig. 5j, p) and friction angle decreased.

It can be seen that a large number of substances with block-like shape were absorbed by particles and covering the surface of particles (Fig. 5l), or rod-like and filling the pores between the particles (Fig. 5o). There were no adsorbates in Fig. 5i–m. Because there are Na_2O_k, Na_2O_c, Al_2O_3, SiO_2 and other components in alumina production liquid (Table 1), many substances can still be adsorbed in the alumina production liquid at 80 days (Fig. 5o); the proportion of adsorbate of **k** and **n** was about 76% and 44%, respectively. In the alumina production liquid, except for the chemical reactions, the adsorption had a significant influence on the shear strength properties. And many pores were filled by adsorbates, particles gathered to the large blocks and arranged very closely, so the attraction between the particles is stronger, and resulting in shear strength parameters increased significantly.

The relationships between microstructural and shear strength parameters

Interaction analysis of the microstructural parameters

To study the interaction of the nine parameters above, each of the 9 parameters of the BP network were used both as the input and the output parameters. A three-layer BP network
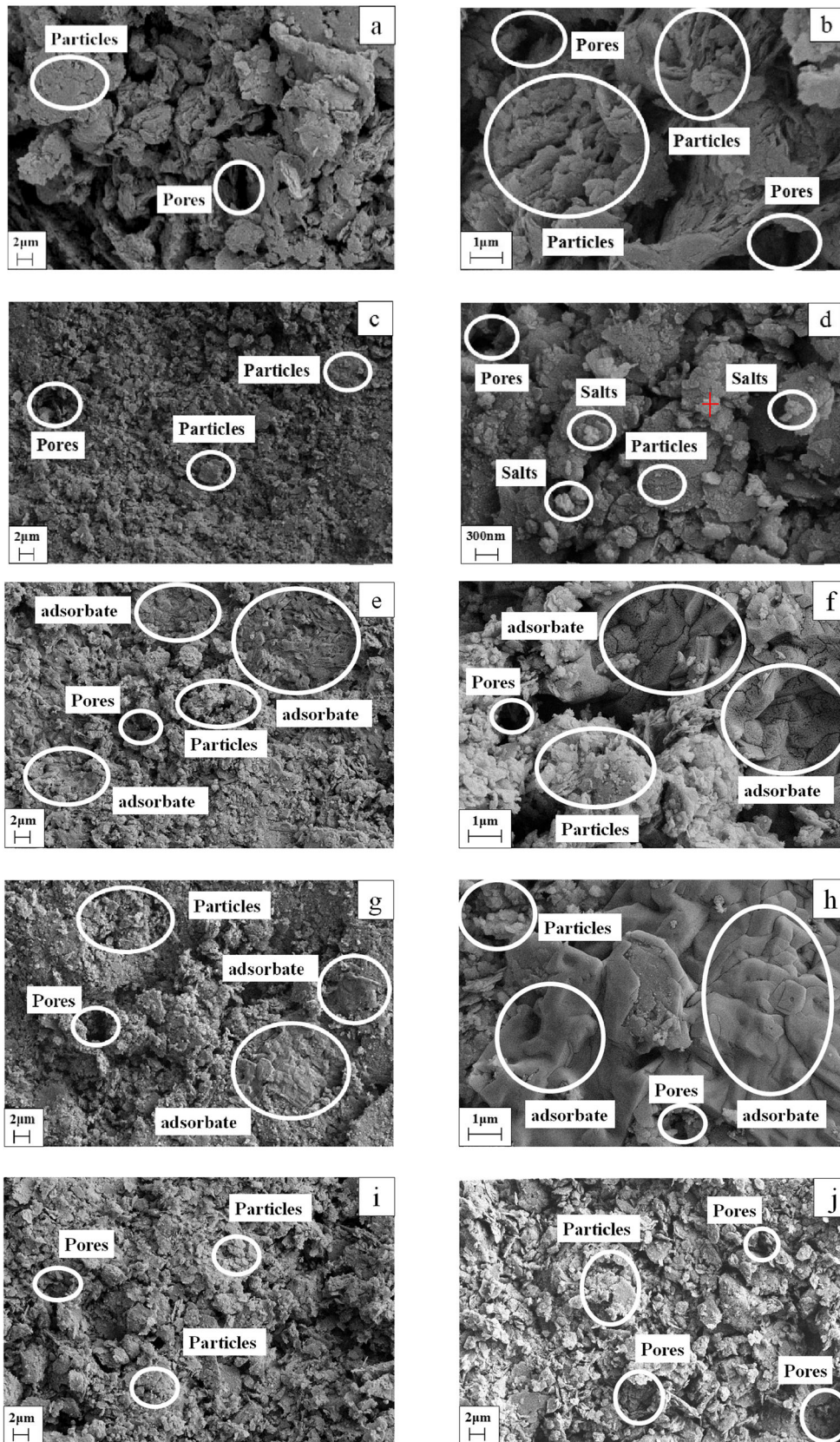
◀ **Fig. 5** SEM images: **a** fresh uncontaminated red clay; **b** the enlarged image of **a**; **c** red clay cured in a concentration of 21% NaOH for 10 days; **d** the enlarged image of **c**; **e** red clay cured in a concentration of 21% NaOH for 20 days; **f** enlarged image of **e**; **g** red clay cured in a concentration of 21% NaOH for 40 days; **h** the enlarged image of **g**; **i** red clay cured in a concentration of 21% NaOH for 80 days; **j** red clay cured in a concentration of 0.7% NaOH for 80 days; **k** red clay cured in the alumina production liquid for 10 days; **l** the enlarged image of **k**; **m** red clay cured in a concentration of 14% NaOH for 80 days; **n** red clay cured in the alumina production liquid for 80 days; **o** the enlarged image of **n**; **p** red clay cured in a concentration of 0.7% NaOH for 10 days; **q** energy-dispersive spectroscopy spectra of the generated salt

was established to obtain the intensities of the interactions between each parameter and all nine parameters (including the specific parameter itself). By trial calculations, the network structural format was determined to be 9–13-9, in which the number of nine parameters (both as input and output) represented the nine microscopic parameters, and the number of hidden nodes was 13. The training target was net.trainParam.goal = 1e−7, while the training rate was net.trainParam.lr = 0.01. The network was converged after 12 training times, and the interaction matrix of the
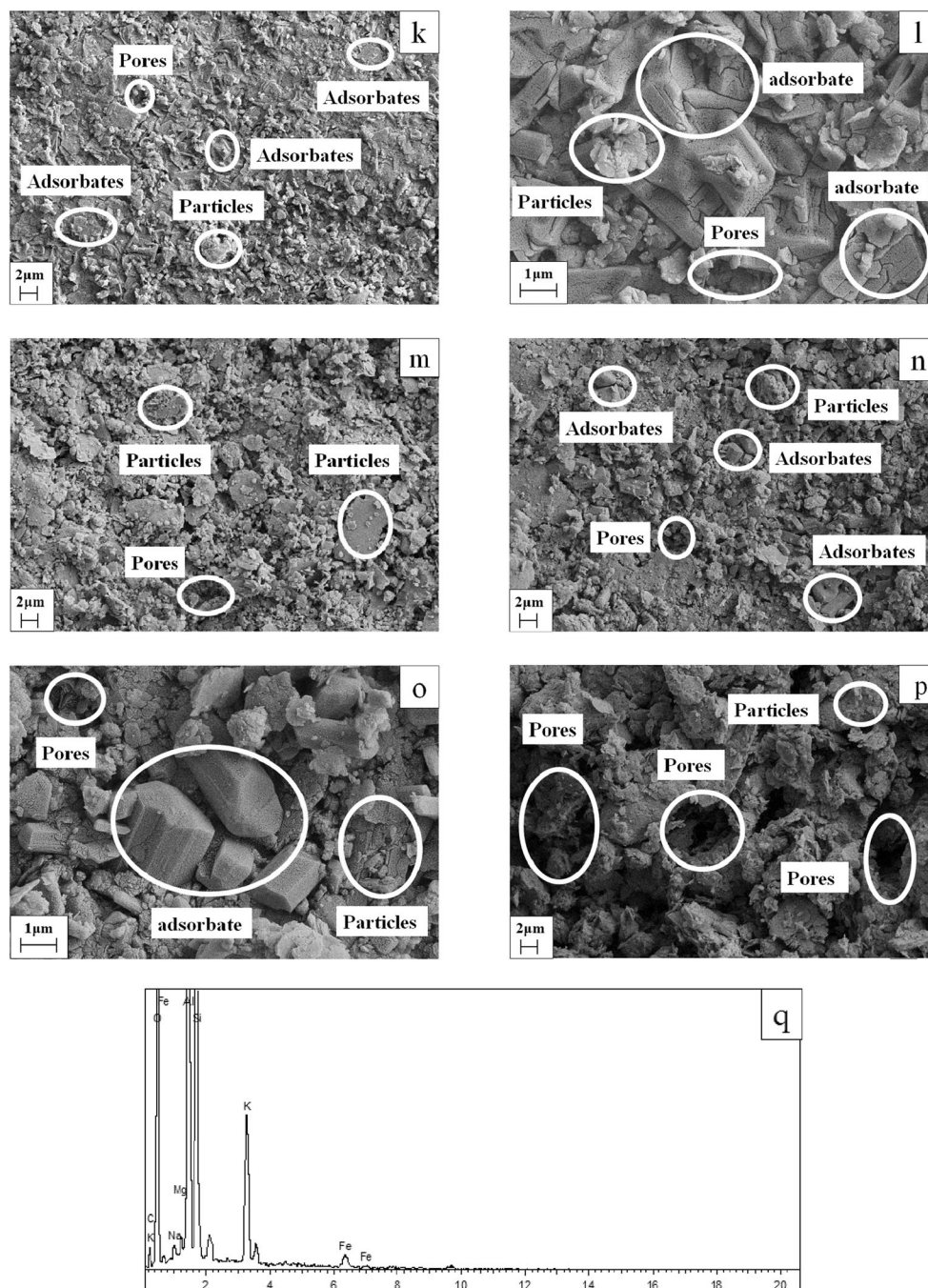

Fig. 5 continued.

Table 5 GRSE of microstructural parameters

Input	Output								
	X_1	X_2	X_3	X_4	X_5	X_6	X_7	X_8	X_9
X_1	1.0000	0.2068	0.0704	0.4270	0.6972	0.3975	0.2951	− 0.8720	− 0.1895
X_2	0.1568	1.0000	− 0.0145	− 0.2225	− 0.1218	0.0334	− 0.2533	0.4923	− 0.0302
X_3	0.0306	− 0.1281	1.0000	− 0.0256	− 0.5087	− 0.2675	0.0175	0.0091	0.2271
X_4	0.4181	0.2560	0.1760	1.0000	− 0.0770	− 0.4992	0.4160	− 0.1266	0.2357
X_5	− 0.3866	− 0.2636	− 0.2405	0.2065	1.0000	0.2210	0.1525	− 0.2246	− 0.4703
X_6	0.2777	0.2962	0.1106	0.0140	0.4714	1.0000	− 0.1422	− 0.5354	− 0.4169
X_7	0.9569	0.8425	0.5726	0.1099	0.5296	0.3101	1.0000	− 0.5247	0.0762
X_8	− 0.2138	− 0.0654	0.0584	0.0106	− 0.1971	− 0.3269	0.2167	1.0000	0.2132
X_9	0.8689	0.5791	0.2851	− 0.4195	− 0.6643	− 0.0553	− 0.4594	− 0.0404	1.0000

microstructural parameters was obtained. The interaction matrix is shown in Table 5.

The upper row in Table 5 is the serial number of the output parameter, and the left column is the serial number of the input parameter. The GRSE is the global relative strength effect (Yang and Zhang 1998). The term $GRSE_{ij}$ ($i = j$) on the diagonal line is 1, indicating that the self-interaction intensity effect of the microscopic parameters is 1. The off-diagonal terms are not 1, in which one parameter's initial change leads to the corresponding changes of other parameters which would eventually cause the initiator's subsequent change. Thus, in a coupled system, the final value of a parameter is probably not the initial value. This concept is unique to the Global Interaction Matrix (GIM) (Ferentinou and Fakir 2018).
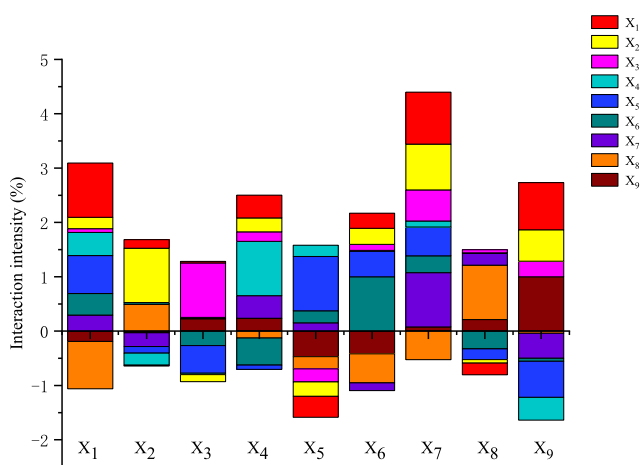
From Table 5, the parameter interaction intensities are not 0. A positive GRSE indicates that the two parameters have

Fig. 6 GRSE interaction matrix of the microstructural parameters. X_1, X_2, X_3, X_4, X_5, X_6, X_7, X_8 and X_9 represent particle morphology fractal dimension, aspect, total number of pores, the ratio of the intra-aggregate pore area, the ratio of the intra-aggregate pore number, total pore area, probability distribution index, probability entropy and number of particles, respectively
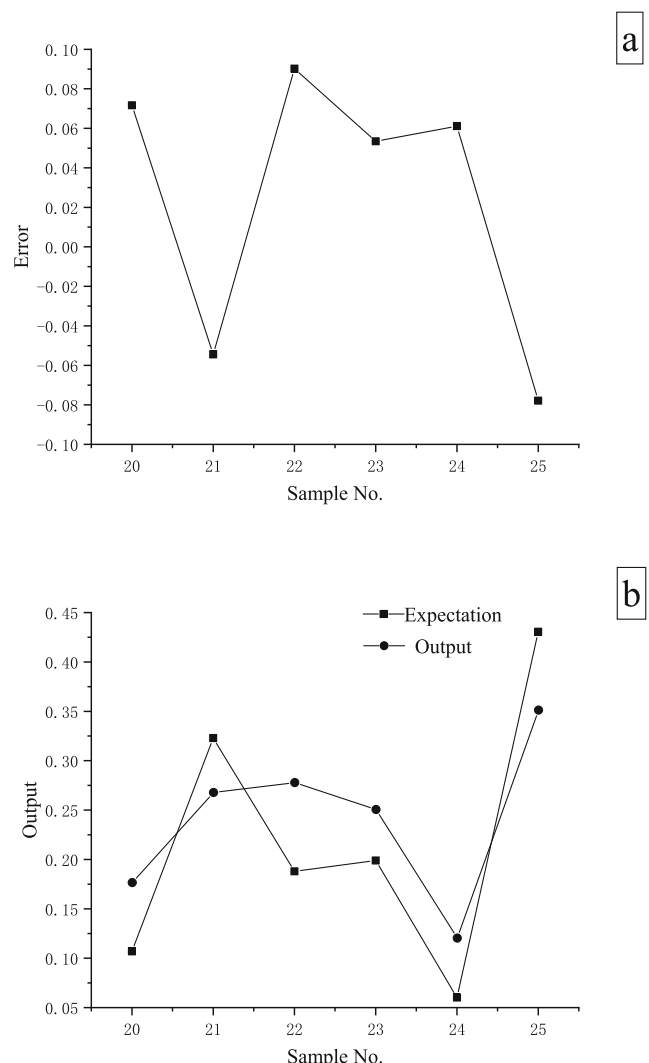
Fig. 7 Error and output of cohesion in the BP network: **a** error of cohesion and **b** output of cohesion

Table 6 GRSE$_i$ of each microcosmic parameter for cohesion

Parameter	X_1	X_2	X_3	X_4	X_5	X_6	X_7	X_8	X_9
GRSE$_i$	0.2801	0.1047	− 0.4091	0.1820	1.000	0.2531	0.8861	− 0.3021	0.7619

positive interactions to each other and vice versa. The larger value of the GRSE means that the more interaction intensity between two parameters, which also indicates that if one value of the microscopic parameter changes, the others also change accordingly and obviously.

To make the GRSE of the microstructural parameters more intuitive, the histogram of the GRSE of the nine parameters is shown in Fig. 6. The interactions between the parameters are not disjoint but coupled intensely; thus, the change in the shear strength parameters depends on the multiple-dimensional interaction of the microscopic parameters. Therefore, the microstructural parameters should not be considered as independent variables; meanwhile, the interaction of microscopic parameters is intense, which could not be ignored.

Interaction of microstructural parameters on cohesion

After several trial calculations, the network structural format was determined to be 9-15-1, and the number 1 represented the cohesion. The BP network model between microscopic parameters and cohesion was established. Figure 7a and b show the error and the output of the cohesion, respectively.

Figure 7a and b show that the maximum error between the output and the expected value is 0.09 (sample 22). The minimum error is 0.053 (sample 23). The relative error is less than 0.1. The output is within acceptance.

Table 6 shows the interaction matrix GRSE$_i$ of the cohesion, where the maximum is 1 (X_5, the ratio of the intra-aggregate pore number) and the minimum is 0.1047 (X_2, aspect). The above nine microscopic parameters also have different influences on the cohesion.

Ma et al. (2006) proposed a method to determine the weight of each involved factor. If the GRSE is given, the weight of the input node's influence on the whole network is U_i, expressed as

$$U_i = \frac{|\text{GRSE}_i|}{\sum |\text{GRSE}_i|} \tag{2}$$

Table 7 represents the weight U_i of each parameter (Eq. 2). Under the interaction of the nine parameters, three parameters greatly affect the cohesion with absolute values above 0.5, which are the ratio of the intra-aggregate pore number, the probability distribution index and the number of particles, respectively. And all of them have positive effects on cohesion. For a soil with the same void ratio and more intra-aggregate pores, then there are fewer inter-aggregate pores. And if the larger the numbers of particles is, the smaller the size of the particle is. Thus, if there are more intra-aggregate pores and smaller-size particles, the soils become more compacted, and the arrangements of particles are more closely. When the compacted soil is subjected to shear stress, the number of particle contacts would increase; therefore, the resistance between the particles would increase, and particle interlocking would be enhanced. This leads to the increase of the internal bond strength and attraction of the particles, so the cohesion increased.

In Fig. 5a, both of the pores and particles size were large (cohesion is 19.06 kPa). In Fig. 5c, both of the numbers of small-size pores and small particles were increased, which resulted in increased cohesion (31.19 kPa). In Fig. 5k, the pore regions were the smallest and most of the pores were intra-aggregate, leading to the largest value of cohesion (135.15 KPa). In Fig. 5p, too many large-size pores were generated and resulted in the cohesion (14.24 KPa). The analyses above provide the evidence of cohesion is influenced significantly by the intra-aggregate pores and small particles.

Interaction of microstructural parameters on friction angle

Using the same method described above, the output layer was changed to the friction angle, and the BP neural

Table 7 Weight U_i of each microscopic parameter for cohesion

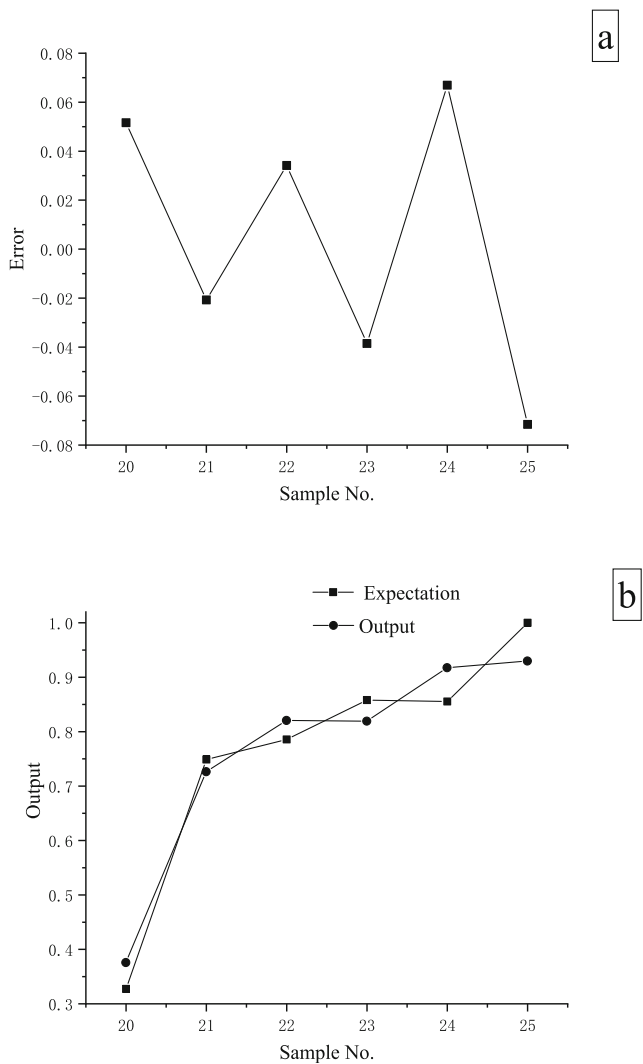| Parameter	X_1	X_2	X_3	X_4	X_5	X_6	X_7	X_8	X_9
U_i	0.0670	0.0251	0.0979	0.0436	0.2393	0.0606	0.2120	0.0723	0.1823

Fig. 8 Error and output of friction angle in the BP network: **a** error of friction angle and **b** output of friction angle

network model between the microscopic parameters and the friction angle was established. Figure 8a, b show the error and output of friction angle, respectively.

Figure 8a and b show that the minimum error between the output and the expected value is 0.02 (sample 21); the maximum error is 0.07 (sample 25). The relative error is less than 0.1. The network output is reasonable.

Table 8 shows that the maximum value of the $GRSE_i$ is 1 (X_1, the particle morphology fractal dimension), and the minimum value is 0.07 (X_4, the ratio of the intra-aggregate pore area).

According to Table 9, there are also three parameters that greatly affect the friction angle: the particle morphology fractal dimension (positive effects), aspect (negative effects) and probability entropy (negative effects). The friction strength of the soil can be divided into sliding and interlock friction. As particles become rounder, they are easier to rotate and provide less resistance to shearing, so the sliding friction decreased. It is also proved by Zelasko et al. (1975) that as the roundness of particles increases, the value of friction angle decrease. When the soil is characterized by a rougher surface, then particles tend to interlock more, thus providing more resistance to shearing, so the more energy consumed for the movement of the particles, and resulting in the sliding friction stronger. This is in agreement with Zelasko et al. (1975) and Janoo (1998) where that as the surface roughness of the soil particles increases, friction angle also increases. Therefore, the contacts between particles increased, and resulting in the orderly arrangements of pores; thus, the value of probability entropy decreased. So the rougher the surfaces of particles, less round shapes of particles and orderly arrangements of pores, will lead to a greater friction angle.

The pores of the red clay were regarded approximately as an equivalent ellipse. Diagrams of the directional distribution of the main axis of the equivalent ellipse were extracted by PCAS software. Comparing the fresh red clay (0 kPa) (Fig. 9a), when the soil was subjected to 300 KPa pressure, the pores were in orderly arrangement (Fig. 9b) (friction angle was 20.9°). The orderly arrangements of pores in Fig. 9c and d were increased obviously, because of the contacts of particles compacted and led to the friction angle increased continually (26.43° and 28.075°, respectively). The orderly arrangements of the pores in Fig. 9e were the most significant, which also indicates that the contacts of particles were the most compacted; thus, the orderly arrangements of pores increased when the soil supported pressure, so the friction angle was the largest (30.6°). Comparing of Fig. 9b, the orderly arrangements of the pores in Fig. 9f was random relatively, and the friction angle was smaller (10.69°).

Table 8 $GRSE_i$ of each microcosmic parameter for the friction angle

Parameter	X_1	X_2	X_3	X_4	X_5	X_6	X_7	X_8	X_9
$GRSE_i$	1.000	−0.5455	−0.3134	0.07	0.1134	−0.2648	−0.2952	−0.4639	0.3018

Table 9 Weight U_i of each microscopic parameter for the friction angle

Parameter	X_1	X_2	X_3	X_4	X_5	X_6	X_7	X_8	X_9
U_i	0.2969	0.1620	0.0931	0.0208	0.0337	0.0786	0.0876	0.1377	0.0896

This also proves that the orderly arrangements of the pores can significantly influence the friction angle above.

Conclusion

The mechanical properties and microstructure of alkaline-contaminated red clay were studied, and based on the RES theory, under the premise of the simultaneous couplings of microscopic parameters, the interaction matrix of microscopic parameters and the relationships between shear strength parameters and the microscopic parameters were investigated. The results presented that:

- Under the attack of alkaline, on the whole, the shear strength parameters of alkaline-contaminated red clay are increased, because the size and area of pores decreased, adsorbates and the formation of salts. Meanwhile, the noticeable dispersing effect of 0.7% NaOH concentration and the generating of large size and area of pores make the friction angle decrease.
- The interaction intensities of the microscopic the parameters are very large and should not be ignored, and need to be investigated in depth.
- More intra-aggregate pores and smaller particles result in higher cohesion. The rougher microstructural surfaces and less round shapes of particles, and orderly arrangements of pores lead to an increased friction angle.
- In this paper, the dependability of the calculated results by the BP network model is proved by microscopic analysis. Future research will be conducted on
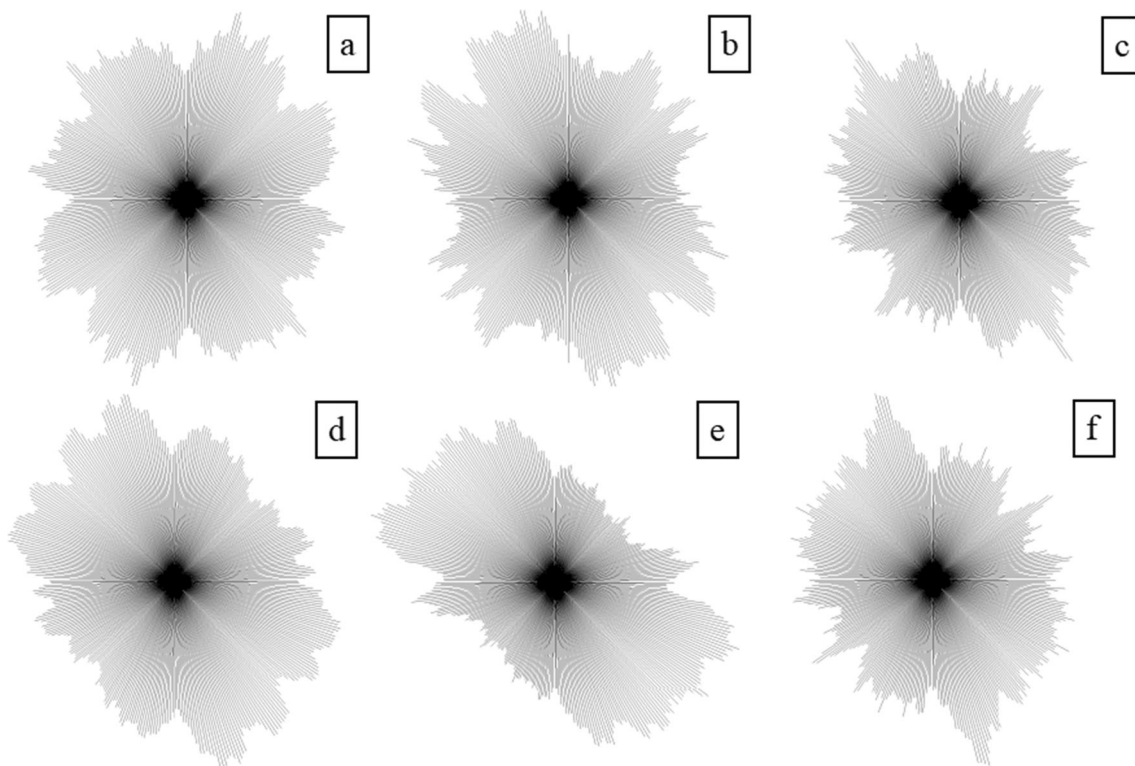

Fig. 9 Diagrams of the directional distribution of the main axis of an equivalent ellipse of the red clay: **a** uncontaminated red clay; 0 kPa; **b** uncontaminated red clay, 300 kPa; **c** red clay cured in a concentration of 21% NaOH for 10 days, 300 kPa; **d** red clay cured in a concentration of 21% NaOH for 80 days, 300 KPa; (e) red clay cured in the alumina production liquid for 80 days, 300 KPa; (f) red clay cured in a concentration of 0.7% NaOH for 10 days, 300 KPa

more soil samples and considering more microscopic parameters to extend the applicability of this model.

References

Anandarajah A, Kuganenthira N (1995) Some aspects of fabric anisotropy of soil. Geotechnique 45(1):69–81. https://doi.org/10.1680/geot.1995.45.1.69

Chavali RVP, Vindula SK, Hari PRP, Babu A, Pillai RJ (2016) Swelling behavior of kaolinitic clays contaminated with alkali solutions: a micro-level study. Appl Clay Sci 135:575–582. https://doi.org/10.1016/j.clay.2016.10.045

Chen YZ, Zhou WH, Liu F, Yi S, Geng X (2019) Microstructure and morphological characterization of lead- contaminated clay with nanoscale zero- valent iron (nZVI) treatment. Eng Geol 256(5): 84–92. https://doi.org/10.1016/j.enggeo.2019.05.001

Chertkov VY (2008) The physical effects of an intra-aggregate structure on soil shrinkage. Geoderma 146(1–2):147–156. https://doi.org/10.1016/j.geoderma.2008.05.011

China Water Power Press (1999) Standard for soil test method (National Standards of the People's Republic of China, GB/T 50123-1999), Beijing (in Chinese)

Cox M, Budhu M (2008) A practical approach to grain shape quantification. Eng Geol 96(1):1–16. https://doi.org/10.1016/j.enggeo.2007.05.005

Cuisinier O, Deneele D, Masrouri F (2009) Shear strength behaviour of compacted clayey soils percolated with an alkaline solution. Eng Geol 108(3–4):177–188. https://doi.org/10.1016/j.enggeo.2009.07.012

Editorial Committee of Handbook of engineering geology (2017) Handbook of engineering geology, 5th edn. China Architecture & Building Press, Beijing

Ferentinou M, Fakir M (2018) Integrating rock engineering systems device and artificial neural networks to predict stability conditions in an open pit. Eng Geol 246:293–309. https://doi.org/10.1016/j.enggeo.2018.10.010

Guizhou Branch of Aluminum Corporation of China (GBAC) (2013a) Method for determination of Al_2O_3 and total alkali content (Q/CHALCO GZ 4106 B03 026-2013), Guiyang (in Chinese)

Guizhou Branch of Aluminum Corporation of China (GBAC) (2013b) Method for determination of Na_2O_k (Q/CHALCO GZ 4106 B03 027-2013), Guiyang (in Chinese)

Huang RQ, Huang J, Ju NP, Li YR (2013) Automated tunnel rock classification using rock engineering systems. Eng Geol 156:20–27. https://doi.org/10.1016/j.enggeo.2013.01.006

Hudson JA (1992) Rock engineering systems theory and practice. Ellis Horwood Limited, London

Hudson JA (2013) A review of rock engineering systems (RES) applications over the last 20 years. Rock characterisation, modelling and engineering design methods-Feng, Hudson, tan (eds) Taylor & Francis Group, London. pp 419–424

Hudson JA, Harrison JP (1992) A new approach to study complete rock engineering problems. Q J Eng Geol Hydrogeol 25:93–105. https://doi.org/10.1144/GSL.QJEG.1992.025.02.03

Janoo VC (1998) Quantification of shape, angularity, and surface texture of base course materials. Cold Regions Research and Engineering Laboratory, Special Report 98–1. https://doi.org/10.1061/40621(254)25

Jiao Y, Hudson JA (1995) The fully-coupled model for rock engineering systems. Int J Rock Mech Min Sci Geomech Abstr 32(5):491–512. https://doi.org/10.1016/0148-9062(95)00038-I

Liu C, Shi B, Zhou J, Tang CS (2011) Quantification and characterization of microporosity by image processing, geometric measurement and statistical method: application on SEM images of clay materials. Appl Clay Sci 54(1):97–106. https://doi.org/10.1016/j.clay.2011.07.022

Ma DX, Guo L, Yang D (2006) Approach to determine weight considering multi-factors interaction influence. Liaoning Tech Univ 25(4): 521–523. (in Chinese). https://doi.org/10.3969/j.issn.1008-0562.2006.04.012

Meulenkamp F, Alvarez Grima M (1999) Application of neural networks for the prediction of the unconfined compressive strength (UCS) from Equotip hardness. Int J Rock Mech Min Sci 36:29–39. https://doi.org/10.1016/S0148-9062(98)00173-9

Ministry of Agriculture of the People's Republic of China (1988) Method for determination of soil organic matter (National Standards of the People's republic of China, GB 9834-88), Beijing (in Chinese)

Ministry of Transport of the People's Republic of China (2007) Test methods of soils for highway engineering (JTG E40-2007), Beijing (in Chinese)

Ministry of Water Resources of the People's Republic of China (1994) Method for determination of silica (dissolved) (SL 91.1-1994), Beijing (in Chinese)

Mulak P, Gaikwad DP, Talhar NR (2016) K-nearest neighbor and boundary cutting algorithm for intrusion detection system. Inf Syst Des Intell Appl 434:269–278. https://doi.org/10.1007/978-81-322-2752-6_26

Pusch R, Weston R (2003) Microstructural stability controls the hydraulic conductivity of smectitic buffer clay. Appl Clay Sci 23(1):35–41. https://doi.org/10.1016/S0169-1317(03)00084-X

Ratnaweera P, Meegoda NJ (1991) Microscopic modeling of shear strength of contaminated soils. Mechanics computing in S & beyond. In: ASCE Engineering Mechanics Speciality Conference

Reddy PHP Sivapullaiah PV (2010) Effect of alkali solution on swell behavior of soils with different mineralogy. Geoflorida. https://doi.org/10.1061/41095(365)273

Reig L, Tashima MM, Borrachero MV, Monzó J, Cheeseman CR, Payá J (2013) Properties and microstructure of alkali-activated red clay brick waste. Constr Build Mater 43:98–106. https://doi.org/10.1016/j.conbuildmat.2013.01.031

Rosli RN, Selamat MR, Ramli MH (2019) Shear strength and permeability properties of lateritic soils from North West Malaysia due to extended compaction. Mater Today: Proc 17:630–639. https://doi.org/10.1016/j.matpr.2019.06.344

Sedira N, Castro-Gomes J, Magrinho M (2018) Study of an alkali-activated binder based on tungsten mining mud and brick powder waste. In: Matbud' 2018- 8th scientific-technical conference on material problems in civil engineering, 163. https://doi.org/10.1051/matecconf/201816306002

Singh VK, Singh D, Singh TN (2001) Prediction of strength properties of some schistose rocks from petrographic properties using artificial neural networks. Int J Rock Mech Min Sci 38(2):269–284. https://doi.org/10.1016/S1365-1609(00)00078-2

Sunil BM, Shrihari S, Nayak S (2009) Shear strength characteristics and chemical characteristics of leachate-contaminated lateritic soil. Eng Geol 106(1–2):20–25. https://doi.org/10.1016/j.enggeo.2008.12.011

Thomas A, Tripathi RK, Yadu LK (2018) A laboratory investigation of soil stabilization using enzyme and alkali-activated ground

granulated blast-furnace slag. Arab J Sci Eng 43:5193–5202. https://doi.org/10.1007/s13369-017-3033-x

Yang Y, Zhang Q (1998) The application of artificial neural networks to rock engineering systems (RES). Int J Rock Mech Min Sci 35(6): 727–745. https://doi.org/10.1016/S0148-9062(97)00339-2

Yin FP, He YF, Wang RM, Wang YP (2005) Application of clay minerals in wastewater treatment. Technol Water Treat 31(5):1–5 (in Chinese)

Zelasko JS, Krizek RJ, Edil TB (1975) Shear behavior of sands as a function of grain characteristics. In: Istanbul Conference Soil Mechanics Found Engineering 1:55–64

Publisher's note Springer Nature remains neutral with regard to jurisdictional claims in published maps and institutional affiliations.